Eur. J. Mech. B - Fluids 20 (2001) 371–398

S0997-7546(01)01133-5/FLA

Heat transfer in a rotor–stator system with a radial inflow

Marc Djaoui, Arthur Dyment *, Roger Debuchy

Université des Sciences et Technologies de Lille I, Laboratoire de Mécanique de Lille, URA CNRS 1441, U.F.R. de Mathématiques Pures et Appliquées, Département de Mécanique Fondamentale, Bâtiment M3, 59655, Villeneuve d'Ascq cedex, France

(Received 22 June 2000; revised 3 December 2000; accepted 3 February 2001)

Abstract – The object of the present work is to produce a better understanding of the flow and heat transfer process occurring in a rotor-stator system, with a low aspect ratio and subjected to a superposed radial inflow. The theoretical approach presented in a previous paper (Debuchy et al., Eur. J. Mech. B-Fluids 17 (6) (1998) 791–810) in the framework of laminar, steady, axisymmetric flow is extended to heat transfer effects. The asymptotic model is simplified and new integral relations including temperature are indicated. The experiments, made in a rotor–stator system with a heated stationary disc, are in agreement with the features of the model in the explored range of the gap ratio, Ekman and Rossby numbers. The data include radial and circumferential mean velocity components, air temperature inside the cavity, temperature and temperature-velocity correlations, and also local Nusselt numbers measured on the stationary disc. The flow structure near the axis is found to be strongly affected by the presence of a superposed inflow, as already observed under isothermal conditions. By contrast, the mean temperature, as well as the correlations concerning velocity and temperature are smaller when a radial inflow is assigned. © 2001 Éditions scientifiques et médicales Elsevier SAS

Nomenclature

a	constant in the relation (17) between t and ru_θ
b	constant in the relations (20)
C_p	specific heat at constant pressure
Ec	Eckert number $= \Omega^2 L^2 [C_p(T_1 - T_0)]^{-1}$
Ek	Ekman number $= [G^2 Re]^{-1}$
G	gap ratio $= H/L$
H	axial clearance between rotor and stator
$I_{m,n}$	integral corresponding to the exponents m and $n = r^{m+1} \int_{-1/2}^{1/2} u_r u_\theta^m (1-t)^n \, \mathrm{d}z$
k	thermal conductivity
L	outer radius of the discs
Ma	Mach number $= \Omega L [(\gamma - 1) C_p T_0]^{-1/2}$
Nu	Nusselt number $= \frac{k_1 H}{k_0 (T_1 - T_0)} \frac{\partial T}{\partial Z}(R, \frac{H}{2})$
P	static pressure
p	dimensionless static pressure $= P[\rho \Omega^2 L^2]^{-1}$
Pr	Prandtl number $= C_p \mu_{0/} k_0$

* Correspondence and reprints.

Q	volume flow rate
q	dimensionless inflow rate or Rossby number $= Q[2\pi\Omega L^2 H]^{-1}$
R	radial coordinate
r	dimensionless radial coordinate $= R/L$
Re	rotational Reynolds number $= \Omega L^2/\nu$
T	temperature
t	dimensionless temperature $= (T - T_0)/(T_1 - T_0)$
$\overline{T'^2}$	temperature correlation
$\overline{t'^2}$	dimensionless temperature correlation $= \overline{T'^2}/(T_1 - T_0)^2$
$U_r,\ U_\theta,\ U_z$	radial, circumferential and axial velocity components, respectively
$u_r,\ u_\theta,\ u_z$	dimensionless radial, circumferential and axial velocity components, respectively $= U_r/\Omega L,\ U_\theta/\Omega L,\ U_z/G\Omega L$
$\overline{U_i' T'}$	temperature-velocity correlations $i, j = r, \theta$
$\overline{u_i' t'}$	dimensionless temperature-velocity correlations $= \overline{U_i' T'}/\Omega L(T_1 - T_0);\ i, j = r, \theta$
$\overline{U_i' U_j'}$	Reynolds stress components $i, j = r, \theta, z$
$\overline{u_i' u_j'}$	dimensionless Reynolds stress components $= \overline{U_i' U_j'}/\Omega^2 L^2;\ i, j = r, \theta, z$
$u_\theta^*,\ u_\theta^{**}$	dimensionless frictional velocities on the stator and on the rotor
w	dimensionless total temperature, $= t + Ec(\frac{u_r^2 + u_\theta^2}{2})$
Z	axial distance from mid clearance
z	dimensionless axial distance $= Z/GL$
α, β	constants in the relations (20)
γ	ratio of specific heats
δ	order of magnitude of the turbulent boundary layer thickness with regards to the clearance
μ	dynamic viscosity
ν	kinematic viscosity
ρ	density
σ	heating factor $= (T_1 - T_0)/T_0$
Ω	angular velocity of the rotor

Subscripts

0	pertaining to conditions outside the cavity
1	pertaining to the stationary disc surface
i	pertaining to the periphery of the cavity

Superscripts

$\sim$	pertaining to the asymptotic solution

1. Introduction

The detailed knowledge of the flow structure and heat transfer process inside rotating cavities [1] is of crucial interest for improving gas-turbine engine performance. Accurate predictions of stresses, growth and durability can be enhanced by knowledge of the turbine disc temperature distribution. In the same way, optimizing disc-cooling efficiency requires insight into the flow circulation and the inherent heat transfer rates. In the current state-of-the-art, the application of computational techniques to the design procedure is difficult because of the complexity of such flows subjected, among other phenomena, to confinement, rotation effects, turbulence and heat transfer. A necessary step consists in the validation of numerical algorithms and turbulence models for idealized geometries, which can be performed only if experimental data are available for comparisons.

Many research programs have been devoted to rotating disc and disc-cavity heat transfer and fluid flow over the past decades. The isothermal flow structure has been investigated extensively. In an enclosed cavity, it was found that the flow structure can be divided into four regimes, two laminar and two turbulent, with or without boundary layers [2]. These regimes have been represented in the G, Re domain and appear to be valid for any rotor–stator system. According to [3] the two laminar regimes are separated by a constant value of $GRe^{1/2}$, larger than one. Actually, it can be checked in the Daily and Nece diagram that the regime with two distinct boundary layers corresponds to $G^2Re > 5$ (*figure 1*). Concerning the turbulent regimes, their common border satisfactorily fits $GRe^{1/5} \approx 0.5$. This result may be obtained if it is assumed that the boundary layers behave as on a single rotating disc and on a stationary disc in a rotating fluid. In both cases the thickness Δ is such that $\frac{\Delta}{R} \sim (\frac{\Omega R^2}{v})^{-1/5}$ [4]. Whence, the two boundary layers merge at the rim when Δ becomes of the order of H, with the result $GRe^{1/5} \sim 1$.

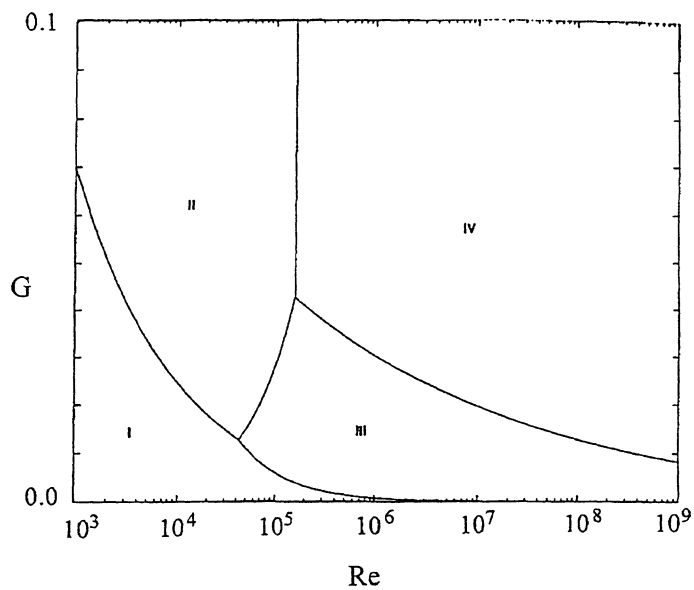

Figure 1. The four regimes of flow in rotor stator systems.

Regime	Clearance	Flow
I	Small	Laminar
II	Large	Laminar
III	Small	Turbulent
IV	Large	Turbulent

More recent experiments brought to evidence that both laminar and turbulent flows can coexist and also that the transition to turbulence first occurs along the stator side [5]. Previous experimental investigations have been of major practical interest, providing data for the assessment of numerical procedures and turbulence models ([6–9]). More recently detailed measurements of mean velocity and of the turbulent flow field have been provided [10]. Experiments published in [1], as well as other configurations such contra-rotating disc and co-rotating disc systems with radial outflow, have involved a numerical analysis [11]. The model tested was a Launder and Sharma low-$Re\,k-\varepsilon$ (L-S). It was shown that the use of a Yap correction term to the dissipation rate equation does not always have a beneficial effect, especially in the case of the rotor–stator cavity with a radial inflow.

As far as heat transfer phenomena are concerned, experiments become more complex and expensive. Measurements of air temperature and heat transfer inside a rotating cavity were performed in [12]: it was found that the gap ratio is a significant parameter for the disk heat transfer process. Measurement of the local heat transfer coefficient were also performed in [13,14]. The experimental data were compared to computational results carried out in [15], obtained with a version of a boundary layer method [16] extended to the case of heat transfer in compressible flow. Comparisons with the experimental data of Northrop and Owen have also been published in [17] using an elliptic solver and a low-Reynolds-number $k-\varepsilon$ turbulence model. Even though it was concluded that some further improvement could be made to predictive capabilities, computed local Nusselt numbers have been found to be within $\pm 10\%$ of measured values, which appears to be sufficiently accurate for engineering design calculations. Radial distributions of rotor heat transfer coefficients have also been obtained using thermochromic liquid crystal coatings with an optical data acquisition system [18]. A combined experimental and computational study of the heat transfer from the heated rotating disk in a rotor–stator system subjected to a radial outflow of cooling air has been performed in [19].

The above review is not exhaustive as the literature is plethoric, and numerous other results can be found in the research monographs [4,20]. However, it appears that there is a lack of available data concerning the temperature and velocity fields inside rotating cavities, as well as fluctuating quantities such as temperature and temperature-velocity correlations. The present work provides an experimental study of the heat transfer process occurring in an unshrouded rotor–stator system subjected to a superposed radial inflow. The flow is characterized by small gap ratio and Ekman number corresponding to a turbulent regime with separate boundary layers. The Rossby number is also small. In addition the velocities and the heating are sufficiently small in order of magnitude to consider the fluid as incompressible and the main dynamical effects dissociated from the heat transfer process. In section 2 the theoretical approach [1] which concerns laminar flow at constant temperature is extended and the asymptotic model is simplified. In section 3, we describe the experimental set-up and the simultaneous temperature and velocity measurement technique. Experimental results for turbulent flow are presented in section 4, including the mean radial and circumferential velocity components, the mean temperature as well as temperature and velocity-temperature correlations, and also heat transfer coefficients on the stator for several values of the Rossby number. The discussion also focuses on the validity of the new quasi-invariants pointed out in section 2 and comparisons between theory and experiments are displayed.

2. Theory

2.1. Physical background

We consider a steady and axisymmetric flow between two parallel coaxial discs, separated by an axial distance H small with regard to their common radius L, one stationary and the other rotating at constant rate Ω (*figure 2*). R is the radial distance from the axis of symmetry, Z the axial distance from the mid-plane.

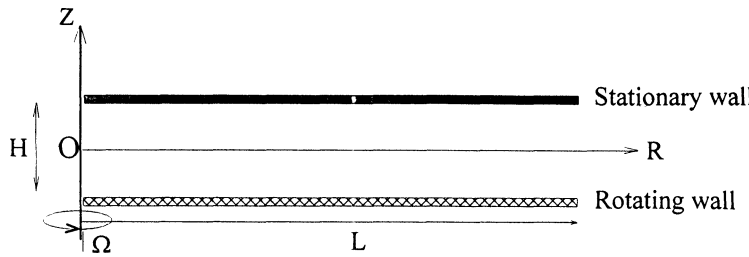

Figure 2. Flow geometry and coordinate system.

U_r, U_θ and U_z are the radial, circumferential and axial velocity components, P is the pressure, ρ the density, T the absolute temperature, μ the viscosity, k the thermal conductivity, C_p the specific heat at constant pressure, γ the ratio of specific heats. The cavity between the discs is open at the periphery: the surrounding gas is at rest in a state characterized by: P_0, T_0, ρ_0, μ_0 and k_0. One of the discs is heated at a constant temperature T_1.

The dimensionless parameters of the problem are the gap ratio G, the Reynolds number Re which may be replaced by the Ekman number Ek, the Prandtl number Pr, the Mach number Ma and the heating factor σ, respectively defined by:

$$\begin{aligned} &G = HL^{-1}, \qquad Re = \rho_0 \Omega L^2 \mu_0^{-1}, \qquad Ek = (Re\, G^2)^{-1}, \\ &Pr = C_p \mu_0 k_0^{-1}, \qquad Ma = \Omega L[(\gamma - 1) C_p T_0]^{-1/2}, \qquad \sigma = (T_1 - T_0) T_0^{-1}. \end{aligned} \tag{1}$$

The scope of our study corresponds to:

$$G \ll 1, \qquad Ek \ll 1, \qquad Pr \sim 1, \qquad \frac{\gamma - 1}{2} Ma^2 \ll \sigma \ll 1. \tag{2}$$

According to the theoretical predictions in laminar flow [3], $G \ll 1$ with $Ek \ll 1$or $Ek \sim 1$ correspond to regimes with dominant convective forces, whereas creeping motion is met for $Ek \gg 1$. Separate boundary layers exist when $Ek \ll 1$.

Assumptions (2) concerning Ma and σ indicate that the temperature variations induced by the centrifugal effect of the rotor motion, which are of the order of $\Omega^2 L^2 / 2C_p = (\gamma - 1) Ma^2 T_0 / 2$, are small with regard to $T_1 - T_0$: in other words the characteristic Eckert number $Ec = \Omega^2 L^2 [C_p (T_1 - T_0)]^{-1} = (\gamma - 1) Ma^2 \sigma^{-1}$ is small. In the same way, the induced pressure variations are of the order of $\rho_0 \Omega^2 L^2 \sim Ma^2 P_0 \ll P_0$. A radial inflow of volume rate Q is ensured from the surrounding fluid through a central axial duct where the pressure is $P_0 - \Delta P_0$, the underpressure ΔP_0 being of the order of $\rho_0 \Omega^2 L^2$. Consequently, the Rossby number $q = Q(2\pi \Omega L^2 H)^{-1}$ is at most of the order of 1. As Ma^2 and σ are small, compressibility and buoyancy can be neglected, with the consequence that the velocity and pressure fields are independent of the temperature, which is to be determined afterwards, once the purely dynamic problem has been solved.

Note that the following procedure can also be used in the case of compressible flow.

2.2. Theoretical analysis

We introduce the following normalized quantities, defined by small letters, being both dimensionless and of order 1:

$$\begin{aligned} &R = Lr, \qquad Z = GLz, \qquad U_r = \Omega L u_r, \qquad U_\theta = \Omega L u_\theta, \qquad U_z = G \Omega L u_z, \\ &P - P_0 = \rho_0 \Omega^2 L^2 p, \qquad T - T_0 = (T_1 - T_0) t. \end{aligned} \tag{3}$$

The conservation of mass and momentum for laminar flow can be expressed as [1]:

$$\frac{\partial}{\partial r}(ru_r) + \frac{\partial}{\partial z}(ru_z) = 0, \tag{4}$$

$$\frac{\partial}{\partial r}(ru_r^2) + \frac{\partial}{\partial z}(ru_r u_z) - u_\theta^2 + r\frac{\partial p}{\partial r} = Ekr\frac{\partial^2 u_r}{\partial z^2}, \tag{5}$$

$$\frac{\partial}{\partial r}(r^2 u_r u_\theta) + \frac{\partial}{\partial z}(r^2 u_\theta u_z) = Ekr^2\frac{\partial^2 u_\theta}{\partial z^2}, \tag{6}$$

$$u_r\frac{\partial u_z}{\partial r} + u_z\frac{\partial u_z}{\partial z} + G^{-2}\frac{\partial p}{\partial z} = Ek\frac{\partial^2 u_z}{\partial z^2}. \tag{7}$$

In the right-hand side of equations (5) to (7), only the dominant terms have been kept.

Usually the equations (5) and (6) are written

$$u_r\frac{\partial u_r}{\partial r} + u_z\frac{\partial u_r}{\partial z} - \frac{u_\theta^2}{r} + \frac{\partial p}{\partial r} = Ek\frac{\partial^2 u_r}{\partial z^2}$$

$$u_r\frac{\partial u_\theta}{\partial r} + u_z\frac{\partial u_\theta}{\partial z} + \frac{u_r u_\theta}{r} = Ek\frac{\partial^2 u_\theta}{\partial z^2}.$$

Multiply the first equation by ru_r, the second by ru_θ, equation (7) by $G^2 ru_z$, and add. The result is

$$ru_r\frac{\partial}{\partial r}\left(\frac{u_r^2+u_\theta^2+G^2u_z^2}{2}+p\right) + ru_z\frac{\partial}{\partial z}\left(\frac{u_r^2+u_\theta^2+G^2u_z^2}{2}+p\right) = Ekr\left(u_r\frac{\partial^2 u_r}{\partial z^2} + u_\theta\frac{\partial^2 u_\theta}{\partial z^2} + G^2u_z\frac{\partial^2 u_z}{\partial z^2}\right),$$

where the terms containing G^2 can be neglected. Then, using (4), this equation becomes:

$$\frac{\partial}{\partial r}\left(ru_r\left(\frac{u_r^2+u_\theta^2}{2}+p\right)\right) + \frac{\partial}{\partial z}\left(ru_z\left(\frac{u_r^2+u_\theta^2}{2}+p\right)\right) = Ekr\left(u_r\frac{\partial^2 u_r}{\partial z^2} + u_\theta\frac{\partial^2 u_\theta}{\partial z^2}\right). \tag{8}$$

Conservation of energy gives:

$$\frac{\partial}{\partial r}\left[ru_r(t-Ec\,p)\right] + \frac{\partial}{\partial z}\left[ru_z(t-Ec\,p)\right] = Ekr\left\{Pr^{-1}\frac{\partial^2 t}{\partial z} + Ec\left[\left(\frac{\partial u_r}{\partial z}\right)^2 + \left(\frac{\partial u_\theta}{\partial z}\right)^2\right]\right\}. \tag{9}$$

On the right-hand side only the dominant terms of thermal diffusion and viscous dissipation have been retained.

Let us add equation (9) to equation (8) multiplied by Ec. Introducing $w = t + Ec(\frac{u_r^2+u_\theta^2}{2})$ we obtain the following equation which can replace (9):

$$\frac{\partial}{\partial r}(ru_r w) + \frac{\partial}{\partial z}(ru_z w) = Ek\,Pr^{-1}\,r\left[\frac{\partial^2 w}{\partial z^2} + Ec(Pr-1)\frac{\partial^2}{\partial z^2}\left(\frac{u_r^2+u_\theta^2}{2}\right)\right]. \tag{10}$$

On the discs the conditions are (the heated disc being the stator):

$$u_r = u_\theta = u_z = 0, \quad t = 1, z = 1/2, \tag{11}$$

$$u_r = u_z = 0, \qquad u_\theta = r, \quad z = -1/2. \tag{12}$$

In the case of prescribed inflow the following integral condition must be fulfilled:

$$r \int_{-1/2}^{1/2} u_r \, \mathrm{d}z = -q. \tag{13}$$

Equations (6), (8) and (10) can be written in the condensed form

$$\frac{\partial}{\partial r}(r u_r \xi) + \frac{\partial}{\partial z}(r, u_z \xi) = Ek\, r \Psi, \tag{14}$$

with ξ in place of ru_θ, $\frac{u_r^2+u_\theta^2}{2} + p$ and w. The function Ψ includes terms proportional to second derivatives in z of the normalized unknowns and to squares of first derivatives.

Let $\tilde{u}_r$, $\tilde{u}_\theta$, $\tilde{u}_z$, $\tilde{p}, \tilde{t}$ and $\tilde{w}$ be the asymptotic solution when going to the limit process $G \to 0$, $Ek \to 0$. Equations (4), (5), (7) and (14) become respectively:

$$\frac{\partial}{\partial r}(r\tilde{u}_r) + \frac{\partial}{\partial z}(r\tilde{u}_z) = 0; \qquad \frac{\partial}{\partial r}\left(r\tilde{u}_r^2\right) + \frac{\partial}{\partial z}(r\tilde{u}_r\tilde{u}_z) - \tilde{u}_\theta^2 + r\frac{\partial \tilde{p}}{\partial r} = 0,$$

$$\frac{\partial \tilde{p}}{\partial z} = 0; \qquad \frac{\partial}{\partial r}(r\tilde{u}_r\tilde{\xi}) + \frac{\partial}{\partial z}(r\tilde{u}_z\tilde{\xi}) = 0,$$

$\tilde{\xi}$ being the limit expression of ξ. According to the last equation, $\frac{\tilde{u}_r^2+\tilde{u}_\theta^2}{2} + \tilde{p}$ and $\tilde{w}$ can be considered as functions of $r\tilde{u}_\theta$.

Previous equations cannot meet all the conditions at the walls with the consequence that dynamic and thermal boundary layers exist, the normalized thickness of which are both of the order of $Ek^{1/2}$ as $Pr \sim 1$. In the central core, i.e. outside the boundary layers, the actual solution coincides with the asymptotic one; in particular $\frac{u_r^2+u_\theta^2}{2} + p$ and w can be considered as functions of ru_θ in the central core.

Due to the assumption $Ec \ll 1$ viscous dissipation might be neglected in equations (9) and (10). However, in the inner part of every boundary layer, close to the walls, the velocity and temperature profiles can be considered as almost linear. Consequently, second derivatives in z are very small so that on the right-hand side of equation (10) the viscous dissipation may be of importance in spite of the weakness of Ec. This occurs in a layer of normalized thickness of the order of $(|Pr-1|Ek\,Ec)^{1/2}$.

For $Pr = 1$ the viscous dissipation is always zero in equation (10), whatever the value of Ec may be. Then (10) becomes

$$\frac{\partial}{\partial r}(r u_r w) + \frac{\partial}{\partial z}(r u_z w) = Ek\, r \frac{\partial^2 w}{\partial z^2} \tag{15}$$

which is exactly the same equation as (6). Therefore w is a function of ru_θ and equation (15), viz.

$$u_r \frac{\partial w}{\partial r} + u_z \frac{\partial w}{\partial z} = Ek \frac{\partial^2 w}{\partial z^2},$$

can be written

$$\frac{\mathrm{d}w}{\mathrm{d}(ru_\theta)}\left[u_r \frac{\partial (ru_\theta)}{\partial r} + u_z \frac{\partial (ru_\theta)}{\partial z}\right] = Ek\left\{\frac{\mathrm{d}w}{\mathrm{d}(ru_\theta)}\frac{\partial^2 (ru_\theta)}{\partial z^2} + \frac{\mathrm{d}^2 w}{\mathrm{d}(ru_\theta)^2}\left[\frac{\partial (ru_\theta)}{\partial z}\right]^2\right\}.$$

Taking (6) into account it remains $Ek\frac{d^2w}{d(ru_\theta)^2} = 0$, then $\frac{d^2w}{d(ru_\theta)^2} = 0$ so that w is a linear function of ru_θ, except in the asymptotic case $Ek = 0$ when this function is arbitrary as the resulting equation is always verified. Consequently $w = d - aru_\theta$, d and a being constants.

The conditions (11) on the stator imply $d = 1$, hence

$$w = 1 - aru_\theta, \tag{16}$$

and the conditions (12) provide the temperature on the rotor:

$$t\left(r, -\frac{1}{2}\right) = 1 - \left(a + \frac{Ec}{2}\right)r^2.$$

As Ec is small we have approximately:

$$t = 1 - aru_\theta, \tag{17}$$

$$t\left(r, -\frac{1}{2}\right) = 1 - ar^2. \tag{18}$$

When Pr is different from 1 w remains a function of ru_θ in the central core with an accuracy of the order of Ek. As the actual value of Pr for air is not far from 1, it may be expected that this function is conveniently approached by (16), so that (17) will still hold approximately.

2.3. The asymptotic solution

The problem for the asymptotic dynamic equations for unshrouded cavities has already been addressed in [1].

For the case realized with no forced throughflow, that we call the 'isolated cavity', because the cavity is closed on the axis side:

$$\tilde{u}_r = 0, \qquad \tilde{u}_\theta = \kappa r, \qquad \tilde{u}_z = 0, \qquad 2\tilde{p} = \kappa^2\left(r^2 - 1\right) \tag{19}$$

with κ constant.

When a radial inflow is assigned, even very small, the solution is a superposition of a shear flow driven by the rotor and a vortex induced by the throughflow: it is recalled in appendix A.

A simplification may be brought by considering the vorticity of the flow. The final model, developed in appendix A, represents a rotor–stator system with given inflow rate q, total energy flux $\tilde{E}$ and peripheral vorticity $\tilde{V}_i$, the gradient of which is zero. $\tilde{E}$ and $\tilde{V}_i$ are defined in appendix A. The velocity and pressure fields are:

$$\begin{aligned}
\frac{\tilde{u}_r}{b} &= -r\sin 2\alpha z - \frac{1}{r}\sin(2\alpha z + \beta),\\
\frac{\tilde{u}_\theta}{b} &= r(\cos 2\alpha z - \cos\alpha) + \frac{1}{r}\cos(2\alpha z + \beta),\\
\frac{\tilde{u}_z}{b} &= \frac{-1}{\alpha}(\cos 2\alpha z - \cos\alpha),\\
\frac{2\tilde{p}}{b^2} &= 1 + \sin^2\alpha - r^2\sin^2\alpha - \frac{1}{r^2},
\end{aligned} \tag{20}$$

so that

$$\frac{1}{2}(\tilde{u}_r^2 + \tilde{u}_\theta^2) + \tilde{p} = b^2 \cos\beta - br\tilde{u}_\theta \cos\alpha. \tag{21}$$

The model depends on the three constants b, α and β connected to the quantities q, $\tilde{E}$ and $\tilde{V}_i$ which have a physical significance (see appendix A).

Concerning the asymptotic expression $\tilde{t}$ of the temperature, we know that it turn out to be a function of $r\tilde{u}_\theta$, as $\tilde{t}$ and $r\tilde{u}_\theta$ satisfy the same equation. According to what has been stated at the end of section 2.2, as $Ek = 0$ and as Pr does not interfere in the asymptotic solution, this function is:

$$\tilde{t} = 1 - ar\tilde{u}_\theta \tag{22}$$

which means that $\tilde{t}$ is a parabolic function of r.

It results from relation (13) that however weak the inflow may be, it is not a small perturbation, at least close to the axis. Consequently, the case corresponding to $q \to 0$ differs from that of the isolated cavity.

All previous results hold in the central core.

Consider now the local Nusselt number on the stator defined by

$$Nu = \frac{k_1 H}{k_0(T_1 - T_0)} \frac{\partial T}{\partial Z}\left(R, \frac{H}{2}\right),$$

i.e.

$$Nu = \frac{k_1}{k_0} \frac{\partial t}{\partial z}\left(r, \frac{1}{2}\right). \tag{23}$$

Then, from relation (17), when $Pr = 1$ is met:

$$Nu = \frac{-ak_1 r}{k_0} \frac{\partial u_\theta}{\partial z}\left(r, \frac{1}{2}\right). \tag{24}$$

The results of the theoretical analysis performed in appendix B are: for the isolated cavity Nu grows as r^2 and the same holds with throughflow in a region adjoining the periphery, whereas close to the axis of the discs Nu varies as $1/r$.

2.4. Integral relations

Similarly to the theoretical results contained in [1], very general quasi-invariants can be obtained by the integration of equation (14) over the gap. At first, taking into account the conditions at the walls, the left-hand side gives $\frac{\mathrm{d}}{\mathrm{d}r}(r \int_{-1/2}^{1/2} u_r \xi \, \mathrm{d}z)$. For the right-hand side, the integration of Ψ in the central core is of order 1. Inside the boundary layers, second derivatives in z and squares of first derivatives are of order Ek^{-1}: integration over the boundary layers gives a result of order $Ek^{1/2}$. After multiplying by Ek, the right-hand side of (14) produces a quantity of order $Ek^{1/2}$. Consequently, relation (25) can be deduced:

$$\frac{\mathrm{d}}{\mathrm{d}r}\left(r \int_{-1/2}^{1/2} u_r \xi \, \mathrm{d}z\right) = \mathrm{O}(Ek^{1/2}). \tag{25}$$

The right-hand side is zero when $\xi = 1$, giving the equation (13).

Obviously, the analogous formula for the asymptotic solution is:

$$\frac{\mathrm{d}}{\mathrm{d}r}\left(r\int_{-1/2}^{1/2}\tilde{u}_r\tilde{\xi}\,\mathrm{d}z\right)=0. \tag{26}$$

Let ϕ be a function of ξ with $\mathrm{d}\phi/\mathrm{d}\xi$ of the order of one. Multiplying (14) by $\mathrm{d}\phi/\mathrm{d}\xi$ leads to

$$\frac{\partial[ru_r\phi]}{\partial r}+\frac{\partial[ru_z\phi]}{\partial z}=Ek\,r\,\Psi\frac{\mathrm{d}\phi}{\mathrm{d}\xi}.$$

Consequently, using the above procedure, a general relation can be obtained:

$$\frac{\mathrm{d}}{\mathrm{d}r}\left(r\int_{-1/2}^{1/2}u_r\phi\,\mathrm{d}z\right)=\mathrm{O}\big(Ek^{1/2}\big). \tag{27}$$

This relation remains valid when ϕ is only a function of ξ in the central core.

Previous results can be generalized for turbulent flows. Equation (6) for the mean flow is

$$\frac{1}{r^2}\frac{\partial}{\partial r}\big(r^2u_ru_\theta\big)+\frac{\partial}{\partial z}(u_\theta u_z)=Ek\frac{\partial^2u_\theta}{\partial z^2}-\frac{1}{G}\frac{\partial}{\partial z}(\overline{u'_\theta u'_z}) \tag{28}$$

with $\Omega^2L^2\overline{u'_\theta u'_z}=\overline{U'_\theta U'_z}$.

Taking into account the conditions (11) to be met at the stator, integration from z to $1/2$ leads to

$$\frac{1}{r^2}\frac{\partial}{\partial r}\left[r^2\int_z^{1/2}u_ru_\theta\,\mathrm{d}z\right]-u_\theta u_z=-\frac{1}{G}u_\theta^{*^2}-Ek\frac{\partial u_\theta}{\partial z}+\frac{1}{G}\overline{u'_\theta u'_z}, \tag{29}$$

where the dimensionless frictional velocity at the wall u_θ^* is defined by

$$\Omega^2L^2u_\theta^{*^2}=-\upsilon\frac{\partial U_\theta}{\partial Z}\left(R,\frac{H}{2}\right),$$

i.e.

$$u_\theta^{*^2}=-\frac{1}{GRe}\frac{\partial u_\theta}{\partial z}\left(r,\frac{1}{2}\right). \tag{30}$$

In equation (29) z is taken inside the boundary layer, but outside the viscous sublayer, so that $Ek\frac{\partial u_\theta}{\partial z}$ is negligible with regards to $\frac{1}{G}u_\theta^{*^2}$. Let δGL be the order of magnitude of the boundary layer thickness. In the left-hand side of equation (29) both terms are of the order of δ (the second one because $u_z\sim\delta$ owing to the equation of conservation of mass). Now, inertia, friction and turbulent forces are of the same order of magnitude, whence:

$$u_\theta^{*^2}\sim\overline{u'_\theta u'_z}\sim G\delta. \tag{31}$$

Exactly the same result holds at the rotor, where the dimensionless frictional velocity is u_θ^{**}.

Integration of equation (29) over the gap gives

$$\frac{1}{r^2}\frac{\mathrm{d}}{\mathrm{d}r}\left[r^2\int_{1/2}^{1/2}u_ru_\theta\,\mathrm{d}z\right]=\frac{1}{G}\big(u_\theta^{**^2}-u_\theta^{*^2}\big),$$

so that $\frac{\mathrm{d}}{\mathrm{d}r}[r^2 \int_{-1/2}^{1/2} u_r u_\theta \,\mathrm{d}z] \sim \delta$, which is similar to (25) with $\xi = ru_\theta$.

When ϕ is a function of ru_θ, equations (4) and (6) allow us to write

$$\frac{\partial}{\partial r}(ru_r\phi) + \frac{\partial}{\partial z}(ru_z\phi) = \left[ru_r\frac{\partial(ru_\theta)}{\partial r} + ru_z\frac{\partial(ru_\theta)}{\partial z}\right]\frac{\mathrm{d}\phi}{\mathrm{d}(ru_\theta)}$$
$$= r^2\left[Ek\frac{\partial^2 u_\theta}{\partial z^2} - \frac{1}{G}\frac{\partial(\overline{u'_\theta u'_z})}{\partial z}\right]\frac{\mathrm{d}\phi}{\mathrm{d}(ru_\theta)},$$

ϕ and $\mathrm{d}\phi/\mathrm{d}(ru_\theta)$ are supposed of order 1. With M, the largest absolute value of all extrema of $\mathrm{d}\phi/\mathrm{d}(ru_\theta)$, we have

$$\frac{1}{r^2}\left[\frac{\partial}{\partial r}(ru_r\phi) + \frac{\partial}{\partial z}(ru_z\phi)\right] < M\left[Ek\frac{\partial^2 u_\theta}{\partial z^2} - \frac{1}{G}\frac{\partial(\overline{u'_\theta u'_z})}{\partial z}\right].$$

The same reasoning as for equation (28) leads to

$$\frac{\mathrm{d}}{\mathrm{d}r}\left[r\int_{-1/2}^{1/2} u_r\phi\,\mathrm{d}z\right] = \mathrm{O}(\delta), \tag{32}$$

a relation similar to (27), but the accuracy of which is lower as the boundary layers are thicker when the flow is turbulent.

In order to check the validity of our approach we consider

$$\frac{\mathrm{d}I_{m,n}}{\mathrm{d}r} = 0(\delta), \quad I_{m,n} = r^{m+1}\int_{-1/2}^{1/2} u_r u_\theta^m (1-t)^n \,\mathrm{d}z. \tag{33}$$

One may notice that $I_{m,0}$ corresponds to the quasi-invariants already expressed under isothermal conditions in [1]. The right-hand side of (33) is exactly zero when $m = n = 0$, with $I_{0,0} = -q$.

When Pr is equal to one the relation (18) is valid and $I_{m,n}$ becomes:

$$I_{m,n} = a^n I_{m+n,0}. \tag{34}$$

The asymptotic solution must satisfy $\mathrm{d}\tilde{I}_{m,n}/\mathrm{d}r = 0$, where $\tilde{I}_{m,n} = r^{m+1}\int_{-1/2}^{1/2} \tilde{u}_r\tilde{u}_\theta^m(1-\tilde{t})^n\,\mathrm{d}z$.

As $2\alpha\tilde{u}_r = \partial\tilde{u}_\theta/\partial z$ we can write $\tilde{I}_{m,n} = \int_{b\cos(\alpha-\beta)}^{b\cos(\alpha+\beta)} (r\tilde{u}_\theta)^m(1-\tilde{t})^n\,\mathrm{d}(r\tilde{u}_\theta)$, which shows that the integrals are independent of r.

If $\tilde{t}$ and $r\tilde{u}_\theta$ are connected by (22) the integrals can be calculated. We have for example:

$$\tilde{I}_{0,1} = \frac{-ab^2}{4\alpha}\sin 2\alpha \sin 2\beta, \qquad \tilde{I}_{0,-1} = \frac{1}{2\alpha a}\ln\left(\frac{\cos(\alpha+\beta)}{\cos(\alpha-\beta)}\right). \tag{35}$$

As already mentioned in [1], the assumptions of steadiness and axisymmetry appear to be questionable when considering the integral relations.

3. Experimental set-up

The experimental apparatus consists of two coaxial horizontal discs 750 mm in diameter separated by an adjustable axial gap as shown in *figure 3*. The lower disc is driven by an electric motor which allows the

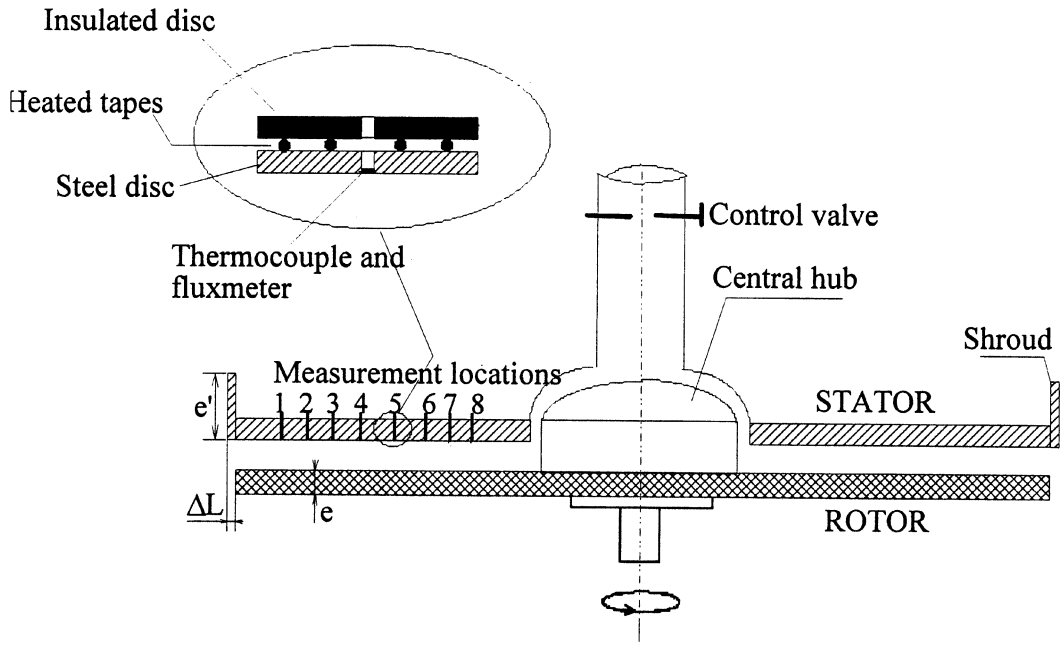

Figure 3. Schematic diagram of the experimental set-up.

rotational speed to be varied up to 2000 rev/min. A rotating central hub, 180 mm in diameter, reproduces the actual layout of turbomachinery and limits the consequences of a possible minor asymmetry of the rotating disc. The perturbation brought about by the hub has only a little influence on the flow except very close to the hub itself [1]. In the present work, the rotor and the hub were not insulated and no thermal boundary conditions were prescribed for these surfaces. To study heat transfer effects, the upper stationary disc was heated by 13 heating tapes with a total power of 5.6 kW, located on the outside face of the disc. The tapes are set along circles concentric to the discs, so that heating does not interfere with the cylindrical symmetry of the boundary conditions, even from the point of view of buoyancy as the discs are horizontal. The device allows an overheating up to 40 degrees with respect to the surrounding atmosphere, the temperature of which is kept close to 297 K. The temperature distribution on the inside face of the disc is adjusted by means of copper-constantan thermocouples connected to electronic temperature controllers. It is to be mentioned that the disc temperature was only measured at the eight locations indicated in *figure 3* which correspond to the following values of r: 0.43, 0.48, 0.53, 0.61, 0.69, 0.77, 0.83, 0.88. No data were obtained near the central hub situated at $r = 0.24$ and at the periphery of the cavity. Eight pellicular fluxmeters, the dimensions of which are $10 \times 10 \times 0.4$ mm, are installed at the above mentioned radial positions. The overall accuracy of the thermocouples and fluxmeters are estimated to be within $\pm 5\%$. A small radial inflow was ensured from the surrounding atmosphere: fluid leaves the cavity through a clearance delimited by the hub and the inner radius of the stator equal to 100 mm. The adjustable volumetric flow rate Q was measured by an Annubar differential-pressure device with an accuracy of 5%.

All the velocity and temperature measurements inside the disc cavity have been performed simultaneously using a specific probe made of three 2.5 μm diameter wires, all situated in the same plane with an angular sensor spacing equal to 120°. Two sensors, connected to a DANTEC 55M25 anemometry device, were used in a constant temperature mode while a cold wire was connected to a DANTEC 56C20 temperature bridge. The probe was introduced through the stator at the same radial locations as those above mentioned, the three wires being situated in a plane parallel to the walls (*figure 4*). It can be moved axially using a DANTEC traversing

system. The probe axis was axially oriented in order to achieve the best spatial resolution and also to give access simultaneously to the mean radial and circumferential velocity components U_r, U_θ, the corresponding turbulent correlations $\overline{U_r'^2}$, $\overline{U_\theta'^2}$ and $\overline{U_r'U_\theta'}$, the mean fluid temperature T, the temperature fluctuations $\overline{T'^2}$ and also the temperature-velocity correlations $\overline{U_r'T'}$ and $\overline{U_\theta'T'}$. With this methodology, only one traverse was necessary for each radial location. The calculation of all previous quantities results from the knowledge of the angular position of the wires and the calibration constants, and of the measurement of the effective velocities, i.e. the velocities to which the wires are sensitive. Processing ensures a good accuracy for the circumferential velocity component which is predominant, but uncertainty exists for the radial velocity and the turbulent correlations because their levels are much smaller. In addition, the radial velocity component results from the difference between two quantities, computed from the effective velocities, which are almost equal.

Calibration of the hot wire probes was carried out in air for several nominal fluid temperatures between 20°C and 65°C, and for velocity of fluid ranging from 5 to 60 m/s which correspond to the conditions for experiments. During the experiments, the measured values of the temperature of fluid were used for applying a correction to the hot-wire anemometer readings obtained from the analysis of the calibration results. It has also been verified that there were no identifiable effects of possible probe interference between the velocity and temperature sensors.

On the one hand, the technique employed in the present work presents some disadvantages over that used in [1]. The specific probe does not have the same type and dimensions as in [1] with the consequence that the probe volume is much larger. In addition, the turbulent correlations including the fluctuation U_z', which are of

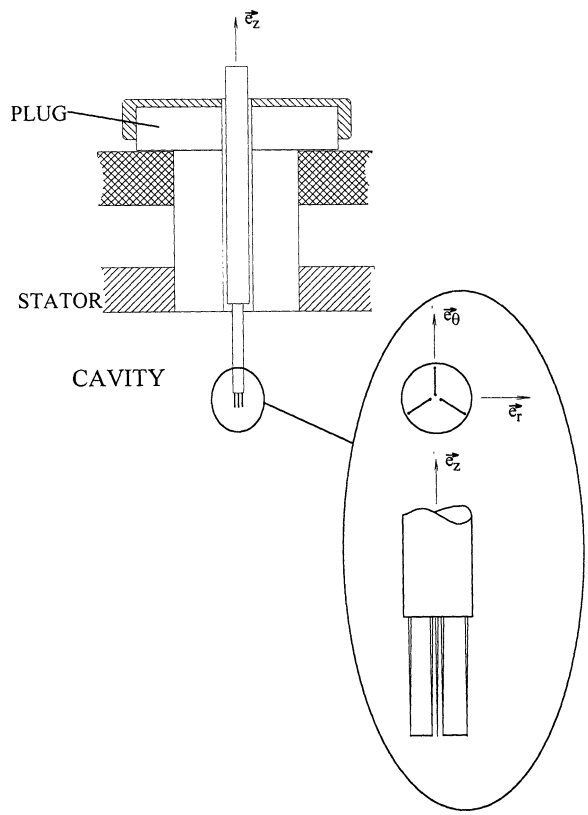

Figure 4. Schematic representation of the anemometer probe.

major importance in the equations governing shear flows, cannot be measured with our device. On the other hand, the simultaneous temperature correction is the main benefit of the technique. Let us also mention that the time averaging has been increased: for all turbulence measurements, 100 000 samples instead of 20 000 in [1] were recorded with a data acquisition rate equal to 20 kHz.

The basic configuration called 'the isolated cavity', without any superposed inflow, was achieved by keeping the flow control valve closed. This situation should correspond to the well known Batchelor model for infinite discs [21]. Now, as the discs are finite, the external peripheral geometry may influence the flow structure and supplementary geometrical parameters need to be considered [22]. Let ΔL be the difference between the stator and rotor radii, e the thickness of the rotor and e' that of the shroud. All these lengths are of the order of H so that the following dimensionless parameters can be introduced: $\lambda = \Delta L \cdot H^{-1}$, $\eta = eH^{-1}$, $\eta' = e'H^{-1}$. In our experiments $\lambda = 0.27$, $\eta = 0.67$ and $\eta' = 4.33$. Obviously, it can be argue that variations of η' do not change significantly the features of the flow and also that η only interferes through the peripheral swirl at $r = 1$. However, experiments made in the case of the isolated cavity have shown that λ is a significant parameter: two distinct flow regimes were observed, the regime corresponding to the infinite discs solution being obtained when λ is not smaller than 0.25 [22]. Taking previous results into account, it may be expected that the value which has been adopted for λ in our experiments with superposed inflow will correspond to the infinite discs case, except in the immediate vicinity of the periphery.

4. Experimental results and discussion

For the results presented below, G was taken equal to 0.08 and the rotational speed was 1500 rev/min, so that Re was fixed to $1.44 \cdot 10^6$ (i.e. $Ek = 1.1 \cdot 10^{-4}$), which corresponds to turbulent flow with separate boundary layers as indicated in *figure 1*. The Rossby number q was varied up to $16.7 \cdot 10^{-3}$, the ambient temperature T_0 was maintained at 297 K and the stator temperature distribution as constant as possible up to $r = 0.88$, with a mean value of T_1 equal to 332 K, corresponding to $\sigma = 0.12 \pm 0.01$, and to $Ec \approx 0.1$. Each configuration required the optimization of the heating tape position in order to achieve the desired temperature distribution, which was one of the main experimental difficulties.

In the manner of the experimental circumferential and radial velocity profiles, plotted respectively in *figures 5* and *6*, the variation of the dimensionless temperature is displayed versus z for the different values of the Rossby number (*figures 7(a)–(c)*) and at different radial locations (*figures 7(d)–(f)*). The first radial location is situated at $r = 0.83$ as we assume that the results may be affected by the inlet conditions and also because the temperature at the stator cannot be correctly controlled in the vicinity of the periphery. As already observed in [1], the case of the isolated cavity is to be distinguished: the fluid rotates as a solid body between the boundary layers. Using a frame of reference rotating with the angular speed of the central core, the Taylor–Proudman theorem may be applied: all components of velocity are independent of z [21]. In the presence of a superposed radial inflow, even infinitesimal, the fluid inside the central core no longer rotates as a solid body: an axial dependence may be observed on the velocity profiles, mainly for the radial component. The core circumferential velocity at mid axis increases with the flow rate, except near the periphery of the cavity where the variations of the Rossby number have few effects (*figure 8*). For the isolated cavity the value $\kappa \approx 0.3$ in (19) is still valid up to $r \approx 0.8$ and the importance of the vortical component is patent when inflow is present. The flow structure is essentially similar to that found under isothermal conditions. The magnitude of u_r and u_θ allows the kinetic terms in the expression of w to be neglected, so that the approximation $t \approx w$ is valid.

The superposed radial inflow also influences the temperature field. *Figure 7* shows that t is nearly constant in the core region, whereas a steep temperature gradient developes in the thermal boundary layers close to the stator [23]. As for the rotor side, both dynamical and thermal boundary layers are too thin to be investigated.

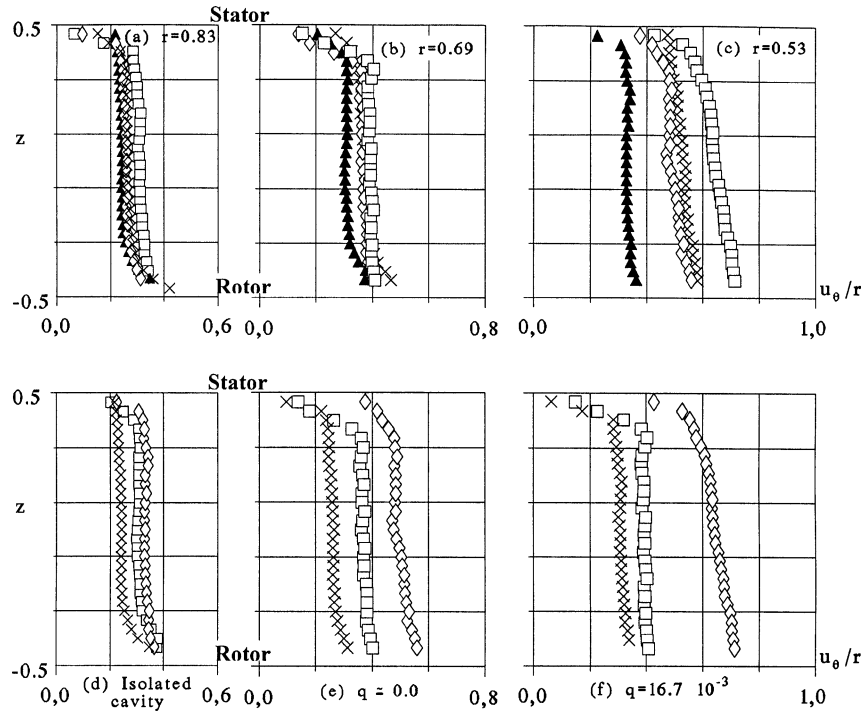

Figure 5. Experimental circumferential velocity profiles. $G = 0.08$, $Re = 1.44\,10^6$, $Ek = 1.1\,10^{-4}$, $\sigma = 0.12$:
(a), (b), (c): ▲ isolated cavity, ◇ $q \approx 0.0$, × $q = 7.2\,10^{-3}$, □ $q = 16.7\,10^{-3}$; (d), (e), (f): × $r = 0.83$, □ $r = 0.69$, ◇ $r = 0.53$.

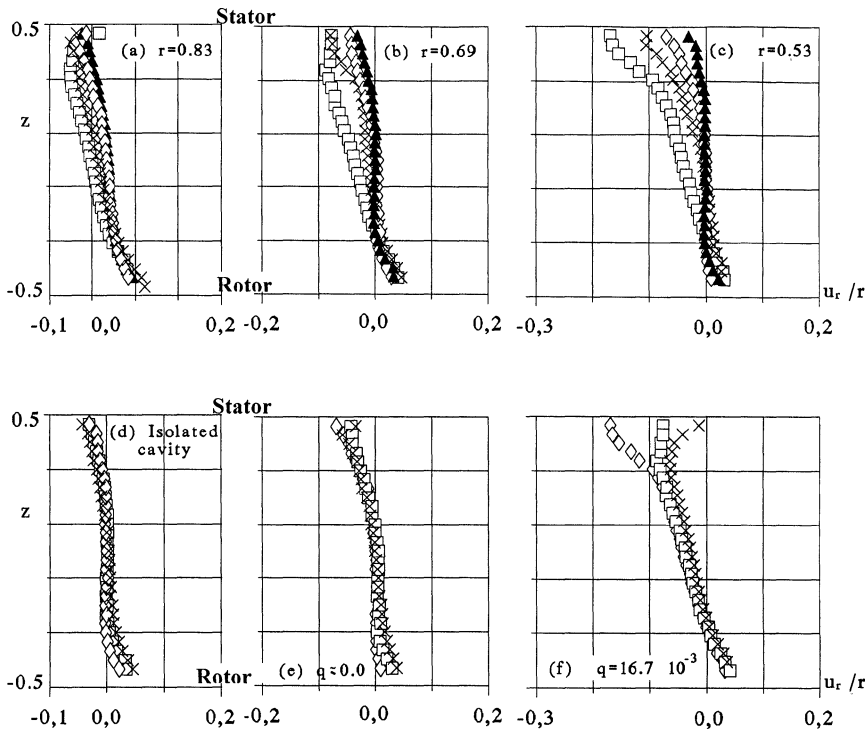

Figure 6. Experimental radial velocity profiles. $G = 0.08$, $Re = 1.44\,10^6$, $Ek = 1.1\,10^{-4}$, $\sigma = 0.12$:
(a), (b), (c): ▲ isolated cavity, ◇ $q \approx 0.0$, × $q = 7.2\,10^{-3}$, □ $q = 16.7\,10^{-3}$; (d), (e), (f): × $r = 0.83$, □ $r = 0.69$, ◇ $r = 0.53$.

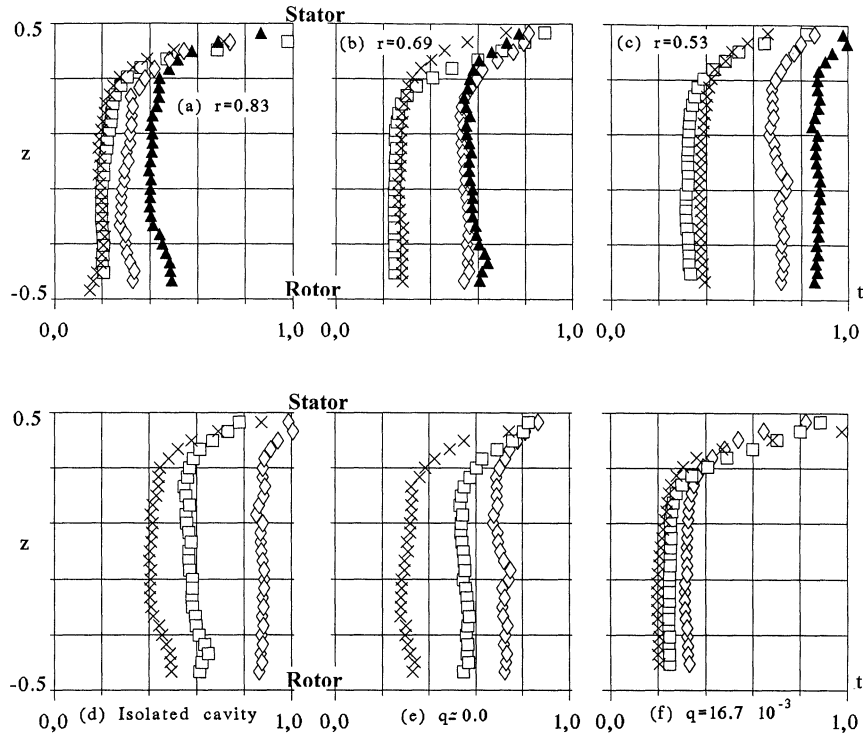

Figure 7. Experimental temperature profiles. $G = 0.08$, $Re = 1.44\,10^6$, $Ek = 1.1\,10^{-4}$, $\sigma = 0.12$:
(a), (b), (c): ▲ isolated cavity, ◇ $q \approx 0.0$, × $q = 7.2\,10^{-3}$, □ $q = 16.7\,10^{-3}$; (d), (e), (f): × $r = 0.83$, □ $r = 0.69$, ◇ $r = 0.53$.

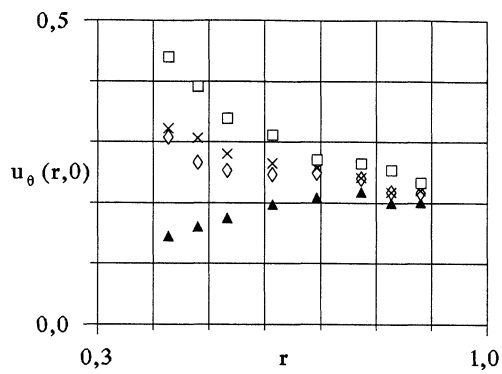

Figure 8. Radial variation of the circumferential velocity at mid-axis. $G = 0.08$, $Re = 1.44\,10^6$, $Ek = 1.1\,10^{-4}$, $\sigma = 0.12$,
▲ isolated cavity, ◇ $q \approx 0.0$, × $q = 7.2\,10^{-3}$, □ $q = 16.7\,10^{-3}$.

Comparison with *figure 5* indicates that the thermal boundary layer thickness at the stator is larger than that of the Ekman boundary layer, which is consistent with the fact that the value of *Pr* is less than 1. Inspection of *figure 9* shows that the level of temperature in the central core depends on the radial location. Near the periphery, throughflow has a limited effect on the dimensionless temperature which is closely linked to the inlet conditions. By contrast, for sufficiently large Rossby numbers the level of t is strongly decreased by the inflow in the region where the vortex is dominant and the temperature profiles tend to gather into a single curve (*figure 7(f)*). For the isolated cavity, as the flow is in solid body rotation at r smaller than 0.7, the temperature of the fluid is close to that of the wall. For the isolated cavity still, and for $q \approx 0.0$, a local increase in temperature

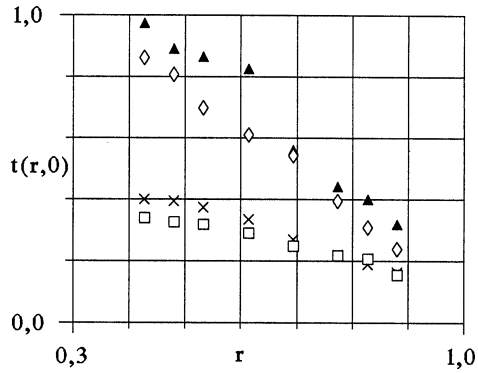

Figure 9. Radial variation of the dimensionless temperature at mid-axis. $G = 0.08$, $Re = 1.44\,10^6$, $Ek = 1.1\,10^{-4}$, $\sigma = 0.12$, ▲ isolated cavity, ◇ $q \approx 0.0$, × $q = 7.2\,10^{-3}$, □ $q = 16.7\,10^{-3}$.

is observed on the side of the rotor: it is the mark of the recirculating heated fluid ($u_r < 0$ in *figure 6*). This temperature bump vanishes when sufficient inflow is present, capturing most of the heated fluid.

To summarize, the already known structure of the velocity field, viz. two boundary layers separated by a central core playing the role of the outer flow, is still valid for the temperature distribution. The increase of temperature undergoes two steps: a first step between the ambient fluid at rest and the core, then a second one, through the boundary layer, leading to the temperature of the stator. For small q and when the cavity is isolated the core and stator temperatures turn closer together as r decreases.

Consider the changes in mean velocity induced by heating. The air which goes through the cavity is a perfect gas subject to relative variations of T of the order of σ. At first, the magnitude of the buoyancy forces per unit volume is $\rho_0 g\sigma$: in the Z momentum equation they are negligible with regards to the inertia forces, of order $\rho_0\Omega^2 H$, leaving unchanged this equation, with the consequence that the pressure remains independent of Z (This result should hold for non horizontal discs). As for the components U_r and U_θ, according to the smallness of the dimensionless pressure variations versus r, of the order of Ma^2, the relative variations of ρ and T are directly opposed. On the other hand, μ varies approximately as T, so that finally the relative variations of ρ and μ are opposed too, with the consequence that changes achieved by the variations of ρ and μ are of opposite sign. As σ is equal to 0.12, one can estimate that changes of U_r and U_θ are at most only of a few percents.

In *figure 10* the effect of inflow on the Nusselt number is displayed. Note that the measured heat fluxes include both convective flux from the stationary disc to the cooling air and the radiative flux from the stator to the rotor. Obviously, as heat transfer is enhanced by convection, an increase in throughflow makes the Nusselt number larger. On the other hand, for given inflow, variations of *Nu* versus r are in connection with the changes in velocity and temperature.

At first, in the particular case of the isolated cavity, Nu increases with r because on the whole the fluid rotates as a solid body and its temperature is not far from that of the heated wall, as already mentioned.

The previous behaviour still holds with inflow but only far from the axis, whereas for small r the vortex plays a dominant part, so that *Nu* increases when the axis is approached.

The change in the variations of Nu observed at $r \approx 0.83$ is certainly due to peripheral effects.

The results represented in *figure 10* are in agreement with the theoretical analysis of appendix B, which is summarized in the end of section 2.3. The behaviour stated when the cavity is isolated is not far from the experimental points which fit approximately the curve $Nu = 150r^2$ up to $r = 0.83$. With inflow the variations

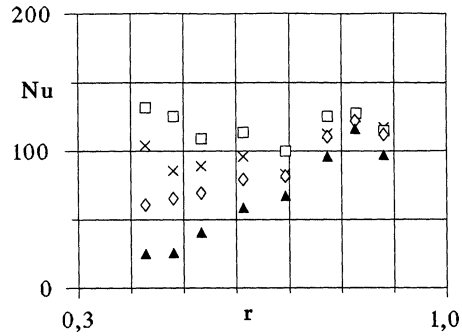

Figure 10. Radial variation of the local Nusselt number on the stator. $G = 0.08$, $Re = 1.44\,10^6$, $Ek = 1.1\,10^{-4}$, $\sigma = 0.12$, ▲ isolated cavity, ◇ $q \approx 0.0$, × $q = 7.2\,10^{-3}$, □ $q = 16.7\,10^{-3}$.

are still in agreement with the theory: the curves drawn for the largest value of q show clearly that Nu decreases for small r and increases when the periphery is approached.

Taking into account the values of T_0 and T_1, $Nu \approx 1.1\frac{\partial t}{\partial z}(r, \frac{1}{2})$ is deduced from formula (23). That gives access to the derivative $\frac{\partial t}{\partial z}(r, \frac{1}{2})$ which is very large, reaching 10^2, a level unforseeable from curves of *figure 7*.

The dimensionless turbulent correlations defined by $\overline{U_i' U_j'} = \Omega^2 L^2 \overline{u_i' u_j'}$ are displayed in *figures 11* to *13* respectively for the isolated cavity, $q \approx 0$ and $q = 16.7 \cdot 10^{-3}$.

Though the heating is not sufficient in magnitude to modify noticeably the mean velocity field it may act on the velocity fluctuations. Most of the theoretical knowledge about this subject is related to parallel flows. Thereby, in our case only a qualitative discussion may be undertaken, based on rough estimates. Remember mainly that the heating of gas flows leads to destabilization due to the dependence of the viscosity of gases on the temperature [24]. Moreover, changes of T act on ρ : the variations of ρ may interfere through gravity forces and centrifugal forces which are apart here, as the discs are horizontal.

The forces resulting from stratification are stabilizing as the heated wall is situated above, except possibly in the regions of bumps mentioned when *figure 7* has been analyzed: however this effect is very weak.

Concerning the motion parallel to the discs, a distinction is to be made between the boundary layer along the stator and the central core, the lower boundary layer being cast aside as the temperature on the wall is unknown.

Similarly to gravity, the body forces associated with rotation are stabilizing when they are directed as the density gradient, which correspond to $\partial\rho/\partial R$ positive.

Inside the stator boundary layer the temperature variations in Z are much larger than the radial ones, producing a steep increase of μ and a decrease of ρ. Now, the velocity being small in the immediate vicinity of the stator the effects of viscosity prevail, promoting instability, hence strenghtening turbulence.

In the central core velocity and temperature are almost independent of Z. As already remarked, the relative variations in ρ and T are directly opposed, and they are at most of the order of σ. As T decreases radially (*figure 9*) ρ increases giving rise to a balance between destabilization induced by the temperature, as if the fluid would be heated from the hub, and stabilization coming from centrifugal body forces. Now, the importance of these forces depends on the magnitude of the tangential velocity which is larger with inflow than when the cavity is isolated (*figure 8*). Consequently, when any inflow is present the influence of density should overcome that of the temperature, involving stabilization, i.e. a damping of the turbulent stresses. In the case of the isolated cavity, as $u_\theta(r, 0)$ grows as r, the destabilizing effect of the temperature should be predominant for small r, leading to an increase of turbulence.

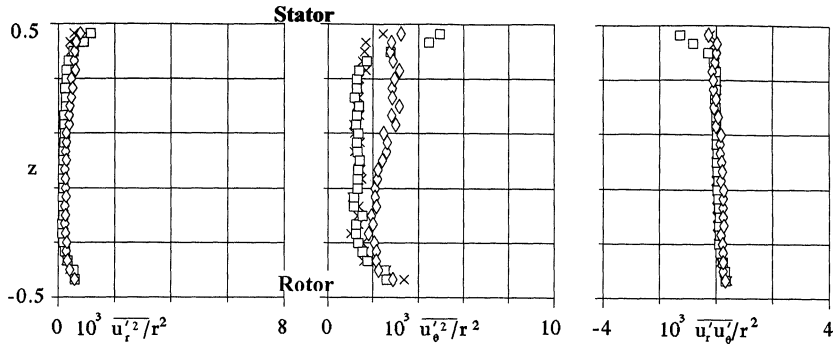

Figure 11. Turbulent correlations for the isolated cavity. $G = 0.08$, $Re = 1.44\,10^6$, $Ek = 1.1\,10^{-4}$, $\sigma = 0.12$: $\times$ $r = 0.83$, $\square$ $r = 0.69$, $\diamond$ $r = 0.53$.

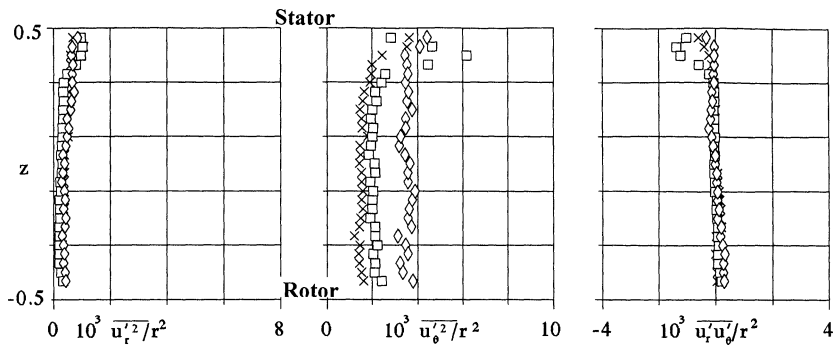

Figure 12. Turbulent correlations in case of radial inflow. $G = 0.08$, $Re = 1.44\,10^6$, $Ek = 1.1\,10^{-4}$, $\sigma = 0.12$, $q \approx 0$, $\times$ $r = 0.83$, $\square$ $r = 0.69$, $\diamond$ $r = 0.53$.

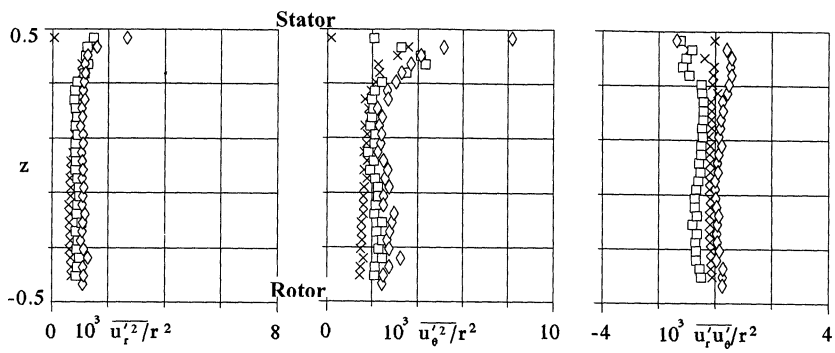

Figure 13. Turbulent correlations in case of radial inflow. $G = 0.08$, $Re = 1.44\,10^6$, $Ek = 1.1\,10^{-4}$, $\sigma = 0.12$, $q = 16.7\,10^{-3}$, $\times$ $r = 0.83$, $\square$ $r = 0.69$, $\diamond$ $r = 0.53$.

The experimental results represented in *figure 14* are in agreement with previous arguments. Peaks of turbulence are observed inside the boundary layer whereas inside the central core damping occurs only in case of sufficient inflow.

The dimensionless temperature correlations $\overline{t'^2}$ and the velocity-temperature correlations $\overline{u'_r t'}$ and $\overline{u'_\theta t'}$ are defined by $\overline{t'^2} = \overline{T'^2}/(T_1 - T_0)^2$, $\overline{u'_r t'} = \overline{U'_r T'}/\Omega L(T_1 - T_0)$, $\overline{u'_\theta t'} = \overline{U'_\theta T'}/\Omega L(T_1 - T_0)$. *Figure 15* shows their variation in the case of the isolated cavity, and *figures 16* and *17* correspond to $q \approx 0$ and $q = 16.7 \cdot 10^{-3}$.

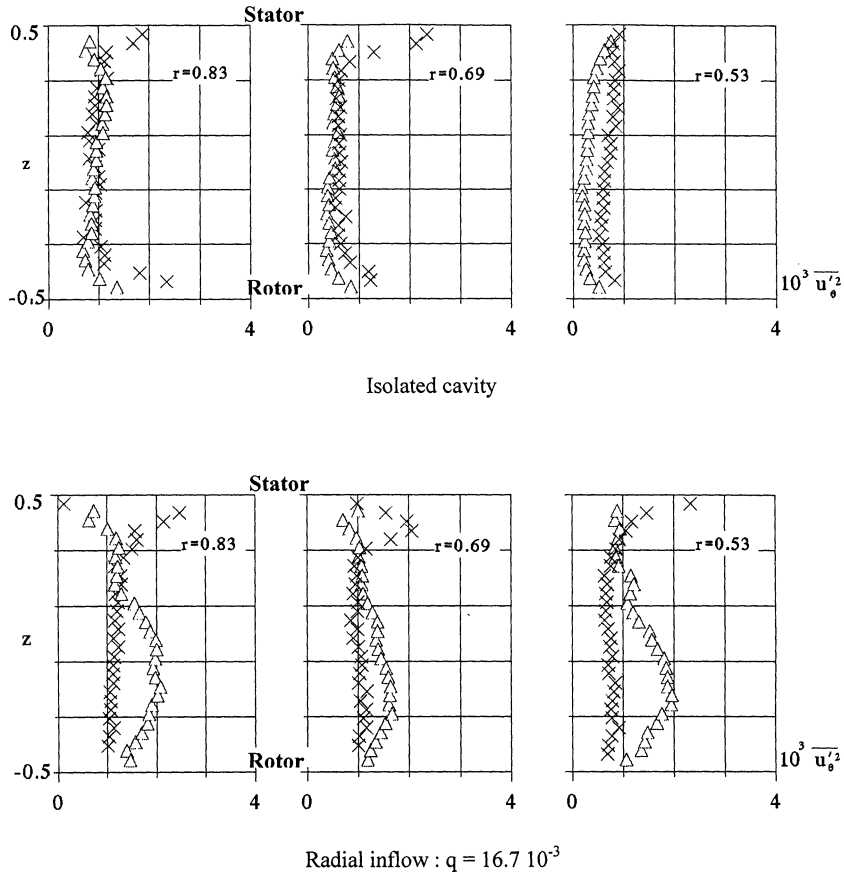

Figure 14. Comparison of the turbulent correlation $\overline{u_\theta'^2}$ with results of reference [1]. $G = 0.08$, $Re = 1.44\,10^6$, $Ek = 1.1\,10^{-4}$, $\times\ \sigma = 0.12$ (present paper), $\triangle\ \sigma = 0$ (values extracted from [1]).

The levels of $\overline{t'^2}$, $\overline{u_r't'}$ and $\overline{u_\theta't'}$ are found to be higher when there is no superposed inflow, with a magnitude of order 10^{-3} in the central core; it decreases with increasing q, the damping being particularly important for $\overline{t'^2}$. Comparison between $q = 16.7 \cdot 10^{-3}$ and the isolated cavity shows that the temperature fluctuations are swept away by the centrifugal effects.

All previous results concerning correlations must be regarded with caution because of the poor accuracy of measurements: no more than trends can be infered from our experimental data.

If all turbulent stresses are of the same order of magnitude as it has been found without heating [1], only their derivatives in z are to be kept in the governing equations. The same holds for the correlations involving temperature. Therefore, in the frame of the present approximation, respectively $r\partial(\overline{u_r'u_z'})/G\partial z$, $r^2\partial(\overline{u_\theta'u_z'})/G\partial z$ and $r\partial(\overline{t'u_z'})/G\partial z$ are to be substracted from the right-hand side of equations (5), (6) and (9) written for the mean turbulent flow. As a consequence the mean velocity profiles are expected to change, but only in the boundary layers because, as already stated in [1], in the central core derivatives in z of all turbulent correlations are close to zero; these changes are too small to be detected.

Power spectral densities, related to output voltage time-history of one of the hot-wire sensors, were obtained in the central core ($z = 0.0$) and also in the stator boundary layer ($z = 0.46$), for both configurations with and without a superposed radial inflow. The analysis of the results showed the absence of any specific low-

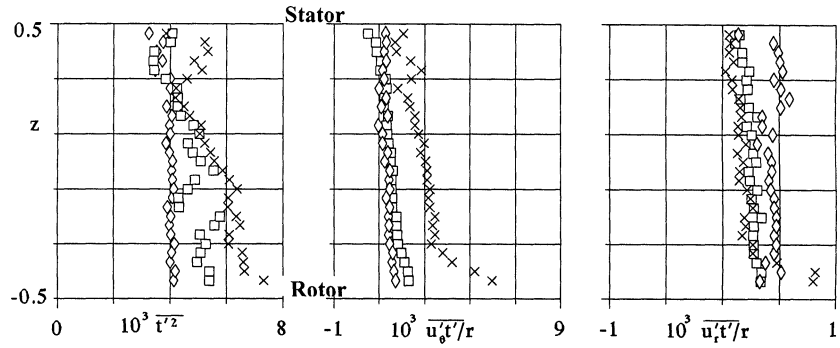

Figure 15. Temperature correlations and velocity-temperature correlations for the isolated cavity. $G = 0.08$, $Re = 1.44\,10^6$, $Ek = 1.1\,10^{-4}$, $\sigma = 0.12$: $\times$ $r = 0.83$, $\square$ $r = 0.69$, $\diamond$ $r = 0.53$.

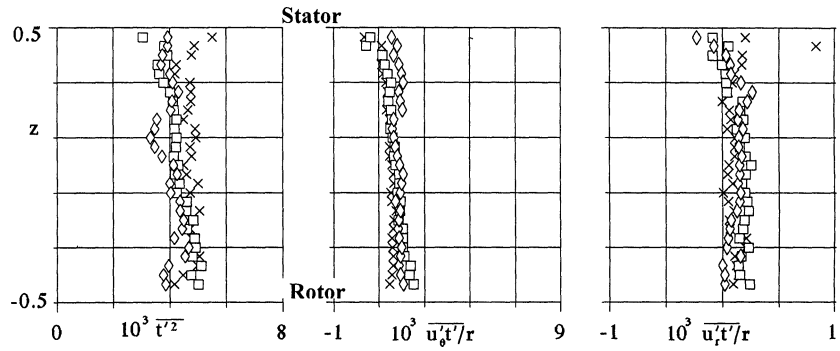

Figure 16. Temperature correlations and velocity-temperature correlations in case of radial inflow. $G = 0.08$, $Re = 1.44\,10^6$, $Ek = 1.1\,10^{-4}$, $\sigma = 0.12$, $q \approx 0$: $\times$ $r = 0.83$, $\square$ $r = 0.69$, $\diamond$ $r = 0.53$.

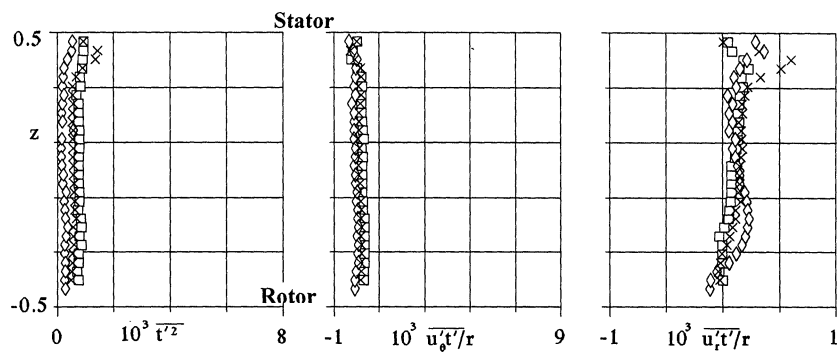

Figure 17. Temperature correlations and velocity-temperature correlations in case of radial inflow. $G = 0.08$, $Re = 1.44\,10^6$, $Ek = 1.1\,10^{-4}$, $\sigma = 0.12$, $q = 16.7\,10^{-3}$: $\times$ $r = 0.83$, $\square$ $r = 0.69$, $\diamond$ $r = 0.53$.

frequency, which indicates that the energy induced by unsteady perturbations can be neglected. This observation reinforces our earlier conclusion following the assessment of the theoretical model in the case of isothermal flow [1]. In the central core, an energy decay process corresponding to the Kolmogorov spectrum can be observed over about one decade for each test case. The only narrow peak in the spectra appears in the stator boundary layer at the frequency of the rotor (25 Hz). This phenomenon is likely to be linked to the fact that the

fluxmeters may stick out slightly from the stator surface, which cannot be totally avoided. Obviously, negligible energy is produced by such a disturbance.

The theoretical relations (17), (20) and (33) are now compared to experimental data corresponding to $q = 16.7 \cdot 10^{-3}$. The integral relations have been obtained in the frame of steady axysimmetrical flow. The function ϕ in (32) being arbitrary, the integral relations are very general, so that, as it has already been observed in [1], if the $I_{m,n}$ are independent of r the assumptions of steadiness and symmetry will be corroborated. The values of $I_{m,n}$ have been computed from formula (33) with the experimental velocity and temperature fields. The accuracy of the results is rather low because, as u_r is partly positive and partly negative, this integral is represented by the difference between two quantities which are almost equal. In addition, for negative values of n or m, a supplementary reason of inaccuracy comes from what happens at the stator where $u_r u_\theta^m (1-t)^n$ becomes indeterminate. However, the mean radial moment of the circumferential momentum corresponding to $m = 1$, $n = 0$, is nearly a constant. The mean value of $-2.63 \cdot 10^{-3}$ is close to that found under isothermal conditions [1]. *Figure 18* shows that the integrals $I_{m,n}$ computed for other values of m and n ($m = 0$ and $n = -1$; $m = -1$ and $n = 0$; $m = 0$ and $n = 1$) are not far from constant.

The validity of the asymptotic solution has been discussed in [1]. Recall that the proposed model for the central core does not have a predictive capacity because the adjustment of the constants b, α and β requires the help of experimental data. According to the fact that the velocity and pressure fields are almost independent of temperature, the values obtained for b, α and β in reference [1], i.e. $b = 0.175$, $\alpha = 17.2°$ and $\beta = 5.5°$ can be taken in the present study. The predicted circumferential and radial velocity profiles, which are not presented here, are in acceptable agreement with the model. As an example the core circumferential velocity at mid axis is displayed in *figure 19*.

The temperature proposed in relation (17) involves the adjustment of the constant a which has been achieved from the experimental distributions. One may observe that a cannot be obtained with the help of a condition at $r = 1$, where air at a temperature close to T_0 enters the cavity, because of peripheral effects, particularly because the temperature on the stator is not kept equal to T_1 up to $r = 1$. What we call here the 'theoretical temperature' has been computed using the experimental values of ru_θ. The best agreement was obtained for $a \approx 3.8$. *Figure 20* shows that relation (17) is in acceptable agreement with the experiments, but only in the central core. With $Pr = 1$ the temperature inside the stator boundary layer is overestimated, producing much larger values of Nu than the actual ones.

The discrepancies observed in the thermal boundary layers between the model and experiments are likely due to the fact that $Pr = 0.72$ instead of 1. Indeed, an inconsistency is met at the stator: when $Pr = 1$ the order

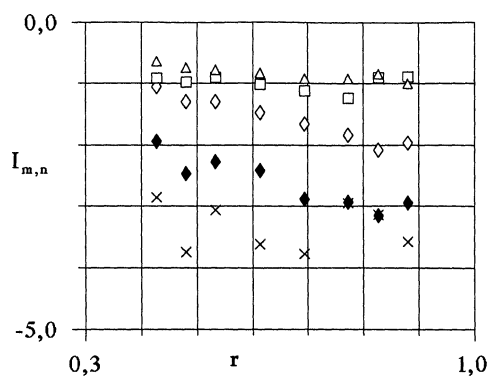

Figure 18. Integrals $I_{m,n}$ of formula (33) resulting from experiments. $G = 0.08$, $Re = 1.44\,10^6$, $Ek = 1.1\,10^{-4}$, $\sigma = 0.12$, $q = 16.7\,10^{-3}$, ♦ $10^3\, I_{1,0}$, □ $10\, I_{-1,0}$, △ $10^2\, I_{0,1}$, × $10^2\, I_{0,-1}$, ◇ $10^3\, I_{1,1}$.

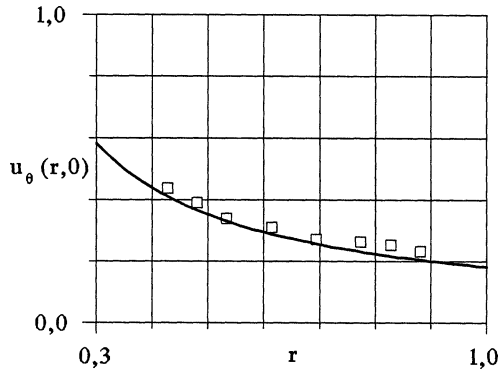

Figure 19. Radial variation of the circumferential velocity at mid-axis. $G = 0.08$, $Re = 1.44\,10^6$, $Ek = 1.1\,10^{-4}$, $\sigma = 0.12$, $q = 16.7\,10^{-3}$, □ experiments, — adjusted theory.

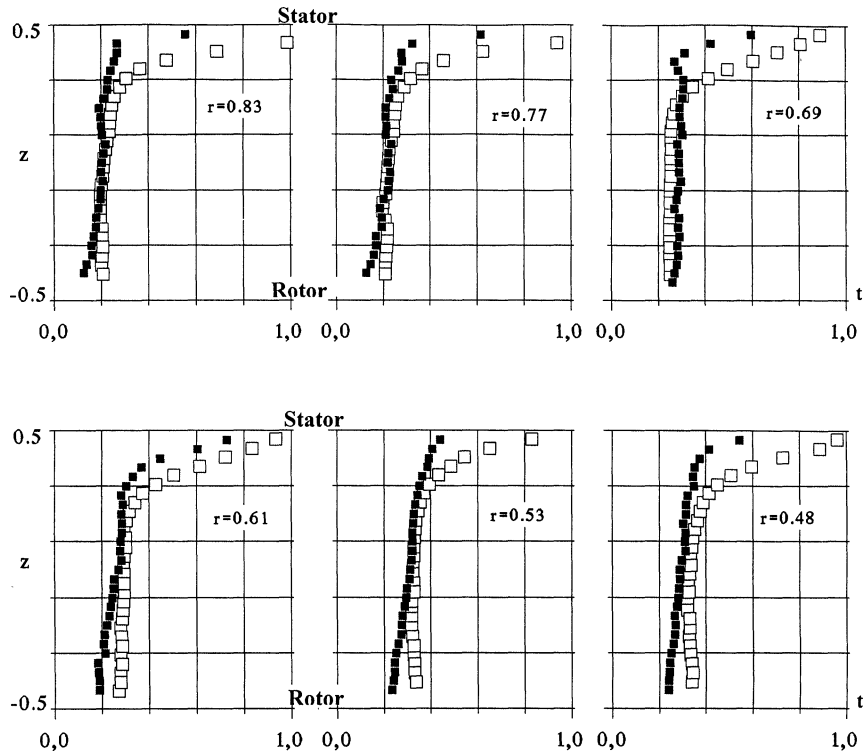

Figure 20. Temperature profiles. $G = 0.08$, $Re = 1.44\,10^6$, $Ek = 1.1\,10^{-4}$, $\sigma = 0.12$, $q = 16.7\,10^{-3}$, □ experiments, ■ theoretical temperature deduced from (17) using the experimental values of ru_θ.

of magnitude of the boundary layer thickness can be linked to Ek and Nu, thanks to (24) and (30), leading to $Nu = \frac{ak_1}{k_0} r G Re\, u_\theta^{*2}$, so that (31) provides roughly $Nu \sim G^2 Re\,\delta$, i.e. $\delta \sim Ek\,Nu$. Taking into account the value of Ek ($Ek \sim 10^{-4}$) and the results of *figure 10* ($Nu \sim 10^{-2}$) we obtain $\delta \sim 10^{-2}$, which means that δ is of the same order as $Ek^{1/2}$ whereas $\delta \gg Ek^{1/2}$ must hold! Moreover, according to *figures 5* to *7* the right value of δ seems to be rather 10^{-1}.

Another surprising phenomenon occurs on the rotor: formula (18) becomes $t(r, -\frac{1}{2}) = 1 - 3.8r^2$ which gives negative values of t for $r \geqslant 0.61$: in this region the rotor seems to be cooled with regard to the ambient air, even very strongly when the periphery is approached. For example at $r = 0.83$, t should be equal to -1.62! Now, if cooling of the external part of the rotor exists, with the consequence that non-negligible thermal gradients are possible inside the rotor, it cannot reach the level indicated by the formula (18).

Indeed, as Pr is different from 1 the formula (17) fails inside the boundary layers, and particularly in the inner domains where viscous dissipation cannot be neglected, as it has been analyzed in section 2.2. All theoretical results based on the assumption $Pr = 1$ are not representative of the actual heat exchanges which take place in the vicinity of the walls.

Concerning the correspondance with the isothermal integrals it has been verified that the relation (34) is admissible and also that the values $\tilde{I}_{0,1} = -0.0104$ and $\tilde{I}_{0,-1} = -0.0261$ deduced from formulas (35) with $a \approx 3.8$, are close to the experimental results presented in *figure 18*. This agreement is a consequence of the weak contribution brought by the boundary layers.

5. Conclusions

Experiments achieved in a heated rotor–stator system subjected to a superposed radial inflow provide numerous data including radial and circumferential mean velocity components, air temperature inside the cavity, temperature and temperature-velocity correlations, as well as local Nusselt numbers on the stationary disc. The study covers a range of dimensionless parameters corresponding to turbulent flow with separate boundary layers, small heating factor and small Rossby numbers.

The main effect of the radial superposed inflow is to enhance the level of the core swirl ratio near the axis, which has already been observed in [1], and at the same time, to increase the heat transfer coefficient on the stationary disc. The effect of heating is analyzed with the help of previous tests conducted in a isothermal environment [1]. As one could forecast small overheating has no important influence on the mean velocity field. All fluctuations are enhanced by a raise of temperature and are lessened when centrifugal forces, induced by the variations of density, act in the opposite direction. Inside the isolated cavity the measured turbulent stresses are little modified with respect to the isothermal flow because of the antagonist actions of temperature and density. On the contrary, the distorting effect of the vortex upon the turbulence tensor observed in [1] in the presence of a radial superposed inflow is attenuated and correlations involving temperature are reduced as the inflow is increased, due to the importance of centrifugal forces connected to the variations of density.

The theoretical analysis presented in [1] is extended to the case of a heated cavity. When the Prandtl number is equal to one, the dimensionless temperature is found to be a linear function of ru_θ.

The validity of the theory is supported by the experimental results as follows:

- the existence of general quasi-invariants is corroborated which warrants the assumptions of steadiness and axisymmetry for the mean flow;
- an acceptable agreement is observed with the theoretical temperature, the discrepancies in the thermal boundary layers being due to the fact that Pr is not equal to 1, so that the model is not able to give accurately account of the behaviour of the air flow close to the walls.

Some features of the model concern laminar flow whereas the actual flow is turbulent; however, on the whole the theory remains valid because convective effects are dominant.

Appendix A

The asymptotic solution presented in [1] is:

$$\begin{aligned}
\tilde{u}_r &= \frac{-cr}{\sin\alpha}\sin 2\alpha z - \frac{b}{r}\sin(2\alpha z+\beta),\\
\tilde{u}_\theta &= \frac{cr}{\sin\alpha}(\cos 2\alpha z - \cos\alpha) + \frac{b}{r}\cos(2\alpha z+\beta),\\
\tilde{u}_z &= \frac{-c}{\alpha\sin\alpha}(\cos 2\alpha z - \cos\alpha),\\
2\tilde{p} &= b^2 + c^2 - c^2r^2 - \frac{b^2}{r^2},
\end{aligned} \tag{A1}$$

where b, c, α and β are constants. It can be easily checked that $2\alpha\tilde{u}_r = \partial\tilde{u}_\theta/\partial z$, $2\alpha r\tilde{u}_z = -\partial(r\tilde{u}_\theta)/\partial r$, and:

$$\frac{1}{2}(\tilde{u}_r^2 + \tilde{u}_\theta^2) + \tilde{p} = \frac{c}{\tan\alpha}\left(\frac{b\cos\beta}{\cos\alpha} - z\tilde{u}_\theta\right). \tag{A2}$$

Global invariants are the mass and total energy fluxes, q and $\tilde{E}$, defined by (13) and

$$r\int_{-1/2}^{1/2}\left[\frac{1}{2}(\tilde{u}_r^2 + \tilde{u}_\theta^2) + \tilde{p}\right]\tilde{u}_r\,\mathrm{d}z = -\tilde{E}. \tag{A3}$$

Taking (A1) and (A2) into account we obtain:

$$\frac{b}{\alpha}\sin\alpha\sin\beta = q, \tag{A4}$$

$$\frac{b^2c}{2\alpha}\sin^2\alpha\sin 2\beta = \tilde{E}. \tag{A5}$$

Let us consider now the distribution of vorticity, which was not analyzed in our previous paper [1]. The vorticity is expressed by

$$\Omega\left[-\frac{1}{G}\frac{\partial u_\theta}{\partial z}\mathbf{e}_r + \left(\frac{1}{G}\frac{\partial u_r}{\partial z} - G\frac{\partial u_z}{\partial r}\right)\mathbf{e}_\theta + \frac{1}{r}\frac{\partial(ru_\theta)}{\partial r}\mathbf{e}_z\right],$$

where $\mathbf{e}_r$, $\mathbf{e}_\theta$ and $\mathbf{e}_z$ are the unit vectors of the cylindrical system of coordinates. It may be observed that when G$\rightarrow$ 0, the vorticity tends to infinity.

Let $\frac{\Omega}{G}V$ be the vorticity amplitude. Obviously, we have for the asymptotic expression $\tilde{V}$ of V:

$$\tilde{V}^2 = \left(\frac{\partial\tilde{u}_r}{\partial z}\right)^2 + \left(\frac{\partial\tilde{u}_\theta}{\partial z}\right)^2.$$

The solution (A1) leads to:

$$\tilde{V}^2 = 4\alpha^2\left(\frac{c^2r^2}{\sin^2\alpha} + \frac{b^2}{r^2} + \frac{2bc\cos\beta}{\sin\alpha}\right), \tag{A6}$$

so that $\tilde{V}$ is independent of z.

The value $\tilde{V}_i$ of $\tilde{V}$ at the inlet represents the initial vorticity:

$$\tilde{V}_i = 2\alpha\left[\left(b - \frac{c}{\sin\alpha}\right)^2 + \frac{2bc}{\sin\alpha}(1+\cos\beta)\right]^{1/2}. \tag{A7}$$

We have

$$\frac{\mathrm{d}(\tilde{V}^2)}{\mathrm{d}r} = 8\alpha^2\left(\frac{c^2 r}{\sin^2\alpha} - \frac{b^2}{r^3}\right) \quad \text{and} \quad \frac{\mathrm{d}^2(\tilde{V}^2)}{\mathrm{d}r^2} = 8\alpha^2\left(\frac{c^2}{\sin^2\alpha} + \frac{3b^2}{r^4}\right).$$

Consequently, the curvature of the graph representing $\tilde{V}^2$ versus r is positive and $\tilde{V}$ is minimum at $r_m = (b\sin\alpha/c)^{1/2}$ with $\tilde{V}_m = 2\alpha[2bc(1+\cos\beta)/\sin\alpha]^{1/2}$. It seems consistent to consider that $\tilde{V}$ increases when the fluid in the central core is advancing towards the axis, which requires $b\sin\alpha \geqslant c$. What is more, if it is assumed that the vorticity varies progressively, with a gradient equal to zero at the periphery, $\mathrm{d}\tilde{V}/\mathrm{d}r = 0$ at $r = 1$, we obtain

$$c = b\sin\alpha, \tag{A8}$$

which allows c to be eliminated from all previous results. Taking (A8) into account the relations (A5), (A6), and (A7) become:

$$\frac{b^3\sin^3\alpha}{2\alpha}\sin 2\beta = \tilde{E}, \tag{A9}$$

$$\frac{\tilde{V}^2}{b^2} = 4\alpha^2\left(r^2 + \frac{1}{r^2} + 2\cos\beta\right), \tag{A10}$$

$$\tilde{V}_i = 2\alpha b\left[2(1+\cos\beta)\right]^{1/2}, \tag{A11}$$

whereas the expressions (A1) of velocities and pressure are changed into (20).

In reference [1] fitting with experiments has led to $c \approx 0.04$ instead of $c \approx 0.052$ given by (A8), resulting from $b = 0.175$ and $\alpha = 17.2°$. This change has no significant influence in our results presented in [1].

Appendix B

For the boundary layer on the stator the axial coordinate and velocity are to be changed into

$$\zeta = Ek^{-1/2}\left(\frac{1}{2} - z\right), \qquad u_\zeta = -Ek^{-1/2}u_z. \tag{B1}$$

The pressure being transmitted from the central core according to the last equation (20), the governing equations are

$$\frac{\partial}{\partial r}(ru_r) + \frac{\partial}{\partial\zeta}(ru_\zeta) = 0, \tag{B2}$$

$$u_r\frac{\partial u_r}{\partial r} + u_\zeta\frac{\partial u_r}{\partial\zeta} - \frac{u_\theta^2}{r} - b^2r^2\sin^2\alpha + \frac{b^2}{r^3} = \frac{\partial^2 u_r}{\partial\zeta^2}, \tag{B3}$$

$$u_r\frac{\partial u_\theta}{\partial r} + u_\zeta\frac{\partial u_\theta}{\partial\zeta} + \frac{u_r u_\theta}{r} = \frac{\partial^2 u_\theta}{\partial\zeta^2} \tag{B4}$$

with the conditions:

$$u_r = u_\theta = u_\zeta = 0, \quad t = 1, \qquad \zeta = 1/2, \tag{B5}$$

$$u_r = \tilde{u}_r\left(r, \frac{1}{2}\right), \qquad u_\theta = \tilde{u}_\theta\left(r, \frac{1}{2}\right), \qquad \zeta \to \infty. \tag{B6}$$

In the region close to the periphery the terms proportional to r are predominant in the pressure gradient and in $\tilde{u}_r$ and $\tilde{u}_\theta$, so that b^2/r^3 can be neglected in (B3) and, according to (20), the matching conditions (B6) become

$$u_r = -br\sin\alpha, \qquad u_\theta = 0, \qquad \zeta \to \infty.$$

It is easy to check that the solution takes the form $u_r = brF(\zeta)$, $u_\theta = brG(\zeta)$, $u_\zeta = bH(\zeta)$, and formula (24) provides

$$Nu = ab\frac{k_1}{k_0}Ek^{-1/2}\frac{\mathrm{d}G(0)}{\mathrm{d}\zeta}r^2. \tag{B7}$$

The same type of solution is valid, whatever r may be, when the cavity is isolated as $\tilde{u}_r$, $\tilde{u}_\theta$ and $\partial\tilde{p}/\partial r$ are in this case proportional to r [1].

On the other hand, for small r the terms proportional to r can be neglected in (B3) and in the expressions of $\tilde{u}_r$ and $\tilde{u}_\theta$ in conditions (B6) which become

$$u_r = \frac{-b}{r}\sin(\alpha+\beta), \qquad u_\theta = \frac{b}{r}\cos(\alpha+\beta), \qquad \zeta \to \infty.$$

This problem is self similar: the single variable is $\eta = b\zeta/r$, which shows that the boundary layer thickness varies as r (whereas it was constant close to the periphery). The approximate expressions of the unknowns are $u_r = \frac{b}{r}f(\eta)$, $u_\theta = \frac{b}{r}g(\eta)$, $u_\zeta = \frac{1}{r}h(\eta)$, and formula (24) provides

$$Nu = ab\frac{k_1}{k_0}Ek^{-1/2}\frac{\mathrm{d}g(0)}{\mathrm{d}\eta}\frac{1}{r}.$$

To summarize, the regime being laminar and Pr equal to one, the Nusselt number on the stator varies asymptotically as r^2 and $1/r$ according as shear flow or vortical flow is dominant.

Acknowledgements

Support for the experimental part of this work was provided by DRET, French Ministry of Defence.

The authors would like express their thanks to the referees for the valuable remarks which have lead to improve the original manuscript.

References

[1] Debuchy R., Dyment A., Muhe H., Micheau P., Radial inflow between a rotating and a stationary disc, Eur. J. Mech. B-Fluids 17 (6) (1998) 791–810.

[2] Daily J.W., Nece R.E., Chamber dimension effects on induced flow and frictional resistance of enclosed rotating disks, ASME J. Basic Eng. 82 (1960) 217–232.

[3] Dyment A., Formulation asymptotique des ćoulements d'un fluide incompressible entre deux disques coaxiaux voisins en rotation, C. R. Acad. Sci. II 292 (1981) 129–132.
[4] Owen J.M., Rogers R.H., Flow and Heat Transfer in Rotating-disc Systems. Volume 1: Rotor–Stator Systems, Research Study Press, Taunton, Somerset, England, 1989.
[5] Itoh M., Yamada Y., Imao S., Gonda M., Experiments on turbulent flow due to an enclosed rotating disk, in: Rodi W., Ganic E.N. (Eds.), Engineering Turbulence Modeling and Experiments, Elsevier, New York, 1990.
[6] Elena L., Schiestel R., Turbulence modeling of rotating confined flows, in: 10th Symp. Turbulent Shear Flows, Pennsylvania State University, USA, 1995.
[7] Elena L., Schiestel R., Turbulence modeling of confined flow in rotating disc systems, AIAA J. 33 (1995) 812–821.
[8] Randriamampianina A., Elena L., Fontaine J.P., Schiestel R., Numerical prediction of laminar, transitional and turbulent flows in shrouded rotor-stator systems, Phys. Fluids 9 (1997) 1696–1713.
[9] Schiestel R., Elena L., Rezoug T., Numerical modelling of turbulent flow and heat transfer in rotating cavities, Numer. Heat Tr. A-Appl. 24 (1993) 45–65.
[10] Cheah S.C., Iacovides H., Jackson D.C., Ji H., Launder B.E., Experimental investigation of enclosed rotor-stator disc flow, J. Exp. Therm. Fluid Sci. 9 (1996) 445–468.
[11] Iacovides H., Nikas K.S., Te Braak M.A.F., Turbulent flow computations in rotating cavities using low-Reynolds-number models, International Gas Turbine and Aeroengine Congress, 1996.
[12] Long C.A., Disk heat transfer in a rotating cavity with an axial throughflow of cooling air, Int. J. Heat Fluid Fl. 15 (1994) 307–316.
[13] Northrop A., Owen J.M., Heat transfer measurements in rotating disc-systems. Part 1. The free disc, Int. J. Heat Fluid Fl. 9 (1988) 19–26.
[14] Northrop A., Owen J.M., Heat transfer measurements in rotating disc-systems. Part 2. The rotating cavity with a radial outflow of cooling air, Int. J. Heat Fluid Fl. 9 (1988) 27–36.
[15] Ong C.L., Owen J.M, Prediction of heat transfer in a rotating cavity with a radial outflow, J. Turbomach. 113 (1991) 115–122.
[16] Ong C.L., Owen J.M., Boundary-layer flows in rotating cavities, J. Turbomach. 111 (1989) 341–348.
[17] Morse A.P., Ong C.L., Computation of heat transfer in rotating cavities using a two-equation model of turbulence, J. Turbomach. 114 (1992) 247–255.
[18] Bunker R.S., Metzger D.E., Witting S., Local heat transfer in turbine disk cavities: Part II – Rotor cooling with radial location injection of coolant, J. Turbomach. 114 (1992) 221–228.
[19] Chen J.-X., Gan X., Owen J.M., Heat transfer in an air-cooled rotor-stator system, J. Turbomach. 118 (1996) 444–451.
[20] Owen J.M., Rogers R.H., Flow and Heat Transfer in Rotating-disc Systems. Volume 2: Rotating Cavities, Research Study Press, Taunton, Somerset, England, 1995.
[21] Batchelor G.K., Note on a class of solutions of the Navier–Stokes equations representing steady rotationally-symmetric flow, Q.J. Mech. Appl. Math. 4 (1951) 29–41.
[22] Djaoui M., Malesys A., Debuchy R., Mise en ́vidence expérimentale de la sensibilité de l'écoulement de type rotor-stator aux effets de bord, C.R. Acad. Sci. IIb 327 (1999) 49–54.
[23] Djaoui M., Debuchy R., Heat transfer between a rotating and a stationary disc with a radial inflow, C.R. Acad. Sci. IIb 326 (1998) 309–314.
[24] Schlichting H., Boundary Layer Theory, 7th ed., McGraw-Hill, 1979.